Earth and Space Science

TECHNICAL REPORTS: METHODS
10.1029/2020EA001247

Coupling Mars Ground and Orbital Views: Generate Viewsheds of Mastcam Images From the Curiosity Rover, Using ArcGIS® and Public Datasets

M. Nachon[1], S. Borges[2], R. C. Ewing[1], F. Rivera-Hernández[3], N. Stein[4], and J. K. Van Beek[5]

[1]Department of Geology and Geophysics, Texas A&M University, College Station, TX, USA, [2]Department of Astronomy and Planetary Sciences—College of Engineering, Forestry, and Natural Sciences, Northern Arizona University, Flagstaff, AZ, USA, [3]Department of Earth Sciences, Dartmouth College, Hanover, NH, USA, [4]Division of Geological and Planetary Sciences, California Institute of Technology, Pasadena, CA, USA, [5]Malin Space Science Systems, San Diego, CA, USA

Key Points:
- Mastcam images from the Curiosity rover are available online but lack a public method to be placed back in the Mars orbital context
- This procedure allows users to generate Mastcam image viewsheds: locate in a map view the Mars terrains visible in Mastcam images
- This procedure uses ArcGIS® and publicly available Mars datasets

Supporting Information:
- Dataset S1
- Dataset S2
- Dataset S3
- Table S1
- Table S2

Correspondence to:
M. Nachon,
mnachon@tamu.edu

Citation:
Nachon, M., Borges, S., Ewing, R. C., Rivera-Hernández, F., Stein, N., & Van Beek, J. K. (2020). Coupling Mars ground and orbital views: Generate viewsheds of Mastcam images from the curiosity rover, using ArcGIS® and public datasets. *Earth and Space Science*, *7*, e2020EA001247. https://doi.org/10.1029/2020EA001247

Received 28 APR 2020
Accepted 18 JUL 2020
Accepted article online 10 AUG 2020

Abstract The Mastcam (Mast Camera) instrument onboard the NASA Curiosity rover provides an exclusive view of Mars: High-resolution color images from Mastcam allow users to study Gale crater's geologic terrains along Curiosity's path. These ground observations complement the spatially broader views of Gale crater provided by spacecrafts from orbit. However, for a given Mastcam image, it can be challenging to locate the corresponding terrains on the orbital view. No method for locating Mastcam images onto orbital images had been made publicly available. The procedure presented here allows users to generate Mastcam image viewsheds, using ArcGIS® software, its built-in Viewshed tool®, and public Mars datasets. This procedure locates onto Mars orbital view the terrains that are observed in a given Mastcam image. Because this procedure uses public datasets, it is applicable to available Mastcam images and to the future ones that will be acquired along the Curiosity rover's path. This procedure can be used by the public to assess scientific questions regarding Martian surface processes and geologic history. In addition, this procedure can be utilized as pedagogic GIS material by the Geosciences or Planetary Sciences communities, for enhancing students' skillsets in GIS and provide students with experience working with datasets from both orbiter and rover Mars missions.

1. Introduction: The Complementary Views of Ground and Orbital Images of Mars

Mars terrain images collected via successive space missions keep refining our view of the red planet. Historically, images collected with spacecrafts (e.g., Mariner 4 flyby in 1965) have offered a spatially extensive view of Mars that later was complemented by higher-resolution images collected from the ground with landers (e.g., Viking 1 landed in 1976 and InSight in 2018) and then rovers (Pathfinder landed in 1997, Spirit and Opportunity in 2004, and Curiosity in 2012). Knowledge about Martian surface processes and the geologic history of the planet have greatly advanced due to our ability to image its surface. Because both orbital and ground views offer complementary information, their coupling is key for optimizing the study and interpretation of geologic terrains.

Orbital images are particularly useful for capturing global, regional, and local contextual information, at a scale that cannot be achieved by a rover's visual range (Stack et al., 2016). In particular, detailed planetary mapping based on high-resolution orbital images provides critical context for more detailed rover measurements. For example, orbital images are used for landing site selection of ground missions and to guide the path and daily operations of rovers such as Curiosity (e.g., Golombek et al., 2012; Stack et al., 2016). Although the entire surface of Mars has been imaged by the Context Camera (CTX) aboard the Mars Reconnaissance Orbiter (MRO) (Dickson et al., 2018), surface coverage by higher resolution cameras encompasses only a small fraction of the surface: The High Resolution Imaging Science Experiment (HiRISE) onboard MRO has mapped ~3% of the surface at a scale from 25 to 60 cm/pixel, between 2006 and 2018 (McEwen et al., 2018). Despite the increased sophistication and spatial resolution of recent orbiter image-based geologic mapping efforts, the interpretation of Mars's geology based exclusively on orbital image datasets still carries considerable uncertainties (e.g., Quinn & Ehlmann, 2019; Stack et al., 2016). In

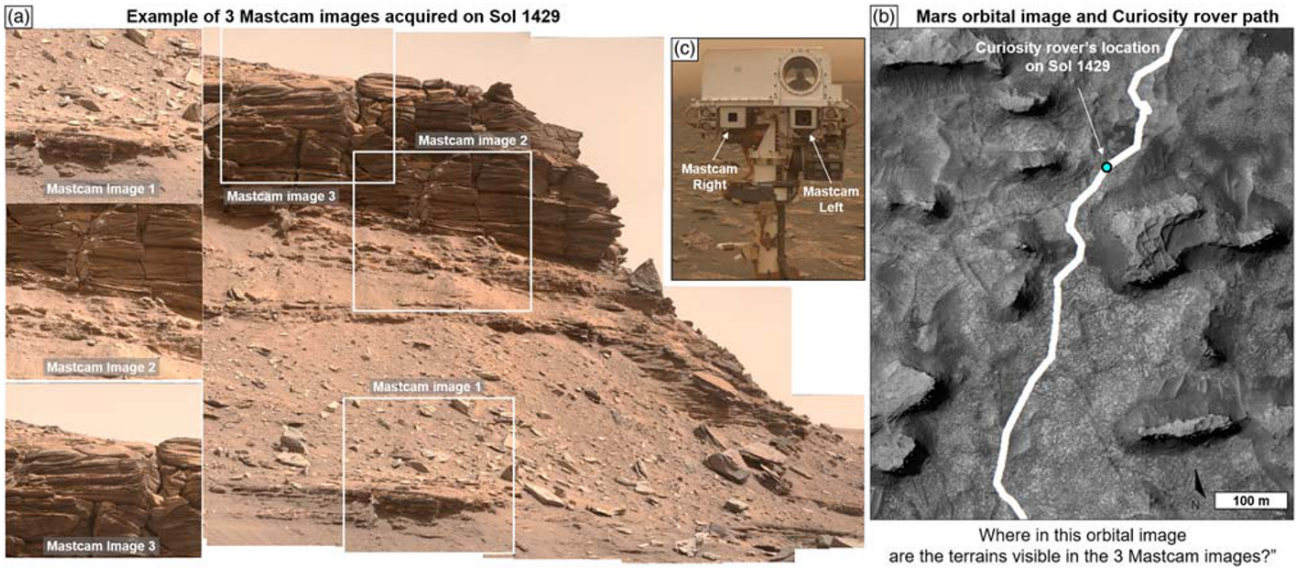

Figure 1. Illustration of the challenge of collocating public Mastcam and orbital images. (a) Example of three Mastcam images (1429MR0070680170702598E01_DRCL, 1429MR0070680060702587E01_DRCL, and 1429MR0070680020702583E01_DRCL) acquired on Sol 1429 and their location within a mosaic of Mastcam images. (b) Mars orbital view of Curiosity rover's location on Sol 1429. (c) Mastcam imagers onboard the Curiosity rover.

particular, the three-dimensional aspects of meter-scale outcrops are difficult to observe in orbital data, which limits the geologic interpretation of the given outcrop.

Ground images, on the other hand, offer a higher-resolution view of Martian terrains (down to the mm-scale) and provide "ground-truth" observations for orbital images. Ground-based images are needed to investigate the small-scale textural characteristics of outcrops, such as grain-size, lithology, internal sedimentary structures, or bedding styles, which are key for making depositional interpretations and paleoenvironmental reconstruction (e.g., Banham et al., 2018; Lewis & Turner, 2019; Stack et al., 2016; Stein et al., 2020). However, in situ observations of the Martian surface are limited to only eight surface mission locations (as of 2020).

In conjunction with each other, orbital and in situ observations provide an ideal, complementary approach to investigate a planetary surface. Such complementary datasets are also used for rover navigation, in particular to obtain precise rover localization (e.g., Parker et al., 2013; Weishu Gong, 2015) and to assist selection of rovers' routes (e.g., minimizing traverses across wheel-damaging terrains; Arvidson et al., 2017).

Among the cameras present onboard the Curiosity rover from the NASA Mars Science Laboratory (MSL) mission, the Mastcam imagers provide an exclusive high-resolution color view of Mars (Figure 1a). Mastcam (Mast Cameras) consists of a pair of color CCD imagers (Mastcam Left and Mastcam Right) mounted on the rover's mast at a height of 1.97 m (Bell et al., 2017; Malin et al., 2017) (Figure 1c). Mastcam Right (MR) has a 100-mm focal length and a field of view of 6.8° × 5.1° and Mastcam Left (ML) has a 34-mm focal length and a field of view of 20° × 15° (Bell et al., 2017; Malin et al., 2017). MR and ML can respectively achieve pixel scales of ~150 and ~450 μm from 2 m (Malin et al., 2017). The Mastcam images allow for fine-scale study of the properties of outcrops and rocks (e.g., Le Deit et al., 2016; Stein et al., 2018), landscape physiography (e.g., Grotzinger et al., 2015), and properties sand (e.g., Bridges et al., 2017; Ewing et al., 2017). They also provide visual context for the compositional analyses from Curiosity's instruments such as ChemCam (Chemistry and Camera) and APXS (Alpha Particle X-Ray Spectrometer) (e.g., Nachon et al., 2017; Thompson et al., 2016; Wiens et al., 2017).

Mastcam images have been used alongside orbital images in several geologic studies of Gale crater's terrains, such as (1) locating and mapping contacts between geologic units or members to establish the stratigraphy of the terrains (e.g., Sheepbed mudstone and overlying Gillespie Lake sandstone in the Yellowknife Bay formation; McLennan et al., 2014); (2) interpreting the geologic origin of outcrops (e.g., eolian Stimson formation; Banham et al., 2018); (3) mapping geologic features too small to be observed from orbit, to determine their

Table 1
Mars Datasets Used and Their Respective Public Sources

Dataset	File name	Source link
Mastcam images and associated labels. See section 2.1	Images are in .IMG format. Labels are in .LBL format.	https://pds-imaging.jpl.nasa.gov/volumes/msl.html under successive volumes (MSLMST_00NN, where NN currently goes from 01 to 24) and in the "DATA" folders.
Gale crater orbital orthophoto mosaic. ("Gale crater mosaic"). See section 2.2	MSL_Gale_Orthophoto_Mosaic_25cm_v3 Original 23 GB. File is in .tif format.	http://astrogeology.usgs.gov/search/map/Mars/MarsScience Laboratory/Mosaics/MSL_Gale_Orthophoto_Mosaic_10m_v3
Gale crater DEM (Digital Elevation Model). See section 2.2	MSL_Gale_DEM_Mosaic_1m_v3 Original 3.6 GB. File is in .tif format.	http://astrogeology.usgs.gov/search/map/Mars/ MarsScienceLaboratory/Mosaics/MSL_Gale_DEM_Mosaic_10m
Rover path localization table. See section 2.2	Table "localized_interp.csv".	https://pds-imaging.jpl.nasa.gov/data/msl/MSLPLC_1XXX/DATA/ LOCALIZATIONS/

spatial and stratigraphic distribution in the different geologic units (e.g., light-toned veins, Nachon et al., 2017; and concretions, Sun et al., 2019). As of January 2020, over 130,000 raw Mastcam images have been acquired with the Curiosity rover (along a 20 km long path) and have been publicly released (Table 1).

Despite the mentioned studies, no method for collocating Mastcam and orbital images has been made publicly available, presenting a roadblock to the combined use of these datasets. As a result, geologic features present within Mastcam images can be challenging to identify within an orbital image of Gale crater, when using only public data. Many Mastcam images contain geologic features tens to hundreds of meters away from the rover's traverse. It is difficult to deduce the spatial scale and location of features in these Mastcam images due to the combination of foreshortening and the lack of reference features. For example, the terrain imaged on Mastcam image 3 (Figure 1a) acquired on Sol (Martian day) 1429 appears to depict the top of a butte; yet, on the orbital image of the rover on that Sol (Figure 1b), the location (how far from the rover and in which direction) and the spatial extent of this terrain are not straightforward to identify.

Herein, we describe a procedure that uses ArcGIS® and publicly available Mars datasets to locate Gale crater terrains seen in Mastcam images into their equivalent orbital view. By successfully correlating in situ and remote observations of Gale crater, we provide the Geoscience and Planetary Science communities access to a methodology for investigating Martian surface processes and geologic history.

2. Datasets and Software

The datasets used are described below and are publicly available online (Table 1).

2.1. Mastcam Datasets

Mastcam images and metadata are posted on the NASA PDS (Planetary Data System) Cartography and Imaging Sciences Node (Table 1) under successive volumes with the conventional name "MSLMST_00NN" (where NN currently goes from 01 to 24), and in the "DATA" folders. Mastcam data are released on a regular schedule (every 4 to 6 months, see http://pds-geosciences.wustl.edu/missions/msl/). It is also available via the MSL Analyst's Notebook (https://an.rsl.wustl.edu/msl/), which provides an interactive interface for visualizing Curiosity's traverse and for accessing data collected by the rover on each Sol and at each visited location.

Mastcam data naming conventions uniquely identify an image or metadata product. The first 4 digits correspond to the Sol during which the image was acquired, and the letters in positions 5 and 6 correspond to the camera name: "MR" for Mastcam Right or "ML" for Mastcam Left (Malin et al., 2013, Table 3.4-1, Section 3.4).

2.1.1. Mastcam Images

The Mastcam images on the PDS are in ".IMG" format (binary image data) (Malin et al., 2013). In this study, we work with Mastcam RDR (Reduced Data Record) images that have been decompressed, radiometrically calibrated, color corrected or contrast stretched, and linearized: This is reflected in their naming convention, where the digits in position 27 to 30 state "DRCL" (Malin et al., 2013). For example, image

1429MR0070680170702598E01_DRCL.IMG is posted online at https://pds-imaging.jpl.nasa.gov/data/msl/MSLMST_0014/DATA/RDR/SURFACE/1429/.

2.1.2. Mastcam Image Metadata

For each Mastcam image, its corresponding metadata is in an associated label (a text file in ".LBL" format) (Malin et al., 2013, Appendix A). Labels include information about images properties and about the location of the rover when the image was acquired.

2.2. Orbital Datasets and Curiosity Rover's Path at Gale Crater

The Gale crater orthophoto mosaic and DEM, which we here use as a basemap for Curiosity rover's path, are available on the Annex of the PDS Cartography & Imaging Sciences Node USGS website (Table 1). The mosaic was assembled by (Calef & Parker, 2016) from HiRISE and CTX data. The associated DEM (Digital Elevation Model) provides the topography of the terrains, at 1 m/pixel postings (Calef & Parker, 2016). It was built from HRSC (High Resolution Stereo Camera) data from the ESA Mars Express spacecraft as well as CTX and HiRISE data from MRO spacecraft (Calef & Parker, 2016). Both the mosaic and the DEM are raster graphics images, in GeoTIFF format.

The Curiosity rover's successive locations on each Sol are publicly available as a plain text table (in CSV format) on the PDS (Table 1), where they are expressed both in rover coordinate frame ("Site" and "Drive," defined as successive position of the rover; MSL Coordinate Systems, 2013) and in the corresponding latitude and longitude values. Here we use the "easting" and "northing" coordinates (in meters). These fields respectively correspond to the longitude and latitude coordinates, in the Equidistant Cylindrical meter units that match the basemap projection (Calef & Parker, 2016).

2.3. ArcGIS® Project and Built-In Viewshed Tool

The ESRI ArcGIS® software (version 10.5) is used here to build an interactive GIS (geographic information system) project that displays the rover path on the orbital mosaic and DEM of Gale crater.

In addition, we use the ArcGIS® built-in Viewshed tool that determines the raster surface locations visible to a set of observer features ["Using Viewshed and Observer Points for visibility analysis" https://desktop.arcgis.com/en/arcmap/10.5/tools/spatial-analyst-toolbox/using-viewshed-and-observer-points-for-visibility.htm]. The Viewshed tool uses the location of an observer on a DEM to identify raster cells that lie within (and outside) of the field of view of the observer at their precise location. Because this tool allows inspection of a limited region of the raster, we use it to identify on the Mars orbital data the terrains that are visible (1) from the position of the rover onto the Gale crater DEM at the time a given Mastcam image was acquired and (2) from the Mastcam imager point of view at that given time (section 3, Step 3). This process highlights on the orbital image the area(s) that correspond to what is observed in the Mastcam image. We term these highlighted areas "Mastcam image viewshed."

3. Mastcam Image Viewshed Procedure: Overview and Illustrative Example

Mastcam image viewsheds locate onto the Gale crater orbital views the terrains that are visible in a given Mastcam image (Figure 2). The main steps of the procedure are (1) gather the Mars public datasets and organize a GIS project to create a map of the Curiosity rover path as seen from orbit; (2) extract and calculate Mastcam image characteristics; (3) incorporate these characteristics into the GIS project and the ArcGIS® Viewshed tool. The description of each procedure step is presented below and also illustrated by an application example, which corresponds to the viewshed production for Mastcam image 1429MR0070680170702598E01_DRCL (image 1 in Figure 1). Through the manuscript, the text corresponding to this application example is in italic bold. Extended descriptions of the procedure steps are provided in the supporting information and referenced along the manuscript.

3.1. Step 1: Gather and Organize Mars Public Datasets

3.1.1. Step 1.1: Download Datasets

All datasets used here are publicly available for download and include the Mastcam data (images and associated labels), Gale crater orthophoto mosaic, Gale crater DEM, and the localization table that contains the coordinates of the Curiosity rover path (section 2 and Table 1). To generate a viewshed, the Mastcam image is not needed per se, only the information included in its label. However, we expect that users interested in generating Mastcam image viewsheds might also want to manipulate the corresponding images. Several

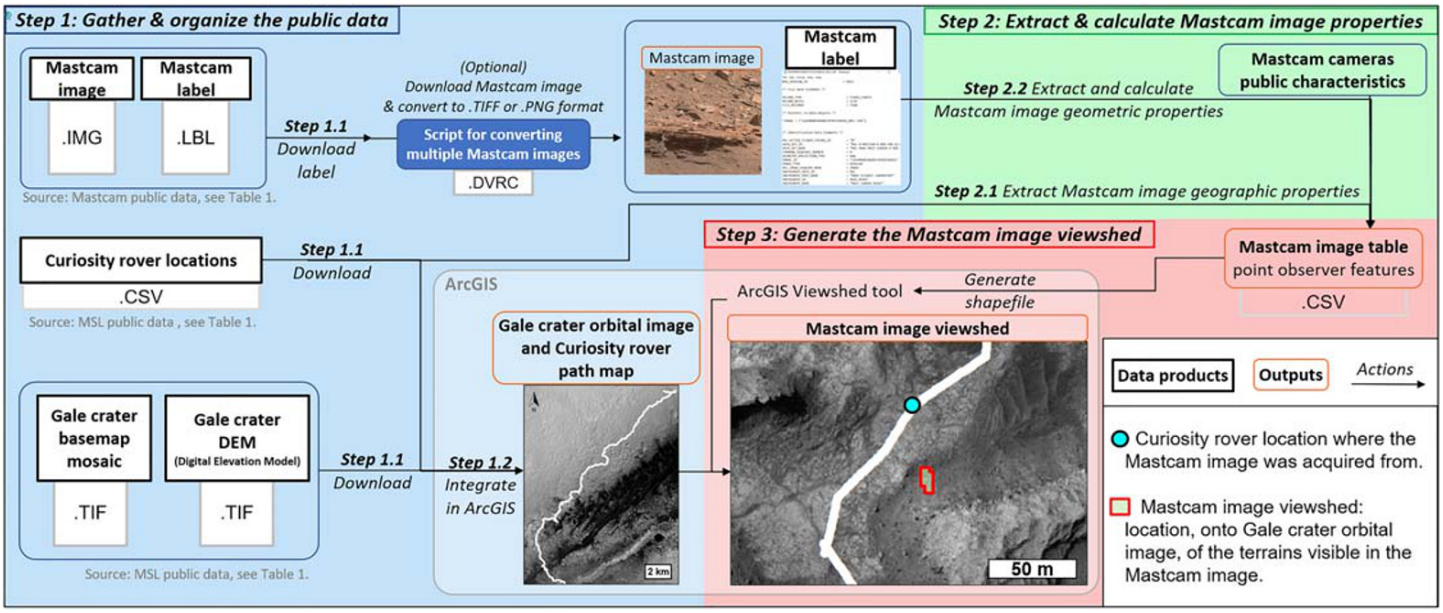

Figure 2. Flowchart of the procedure to generate a Mastcam image viewshed in ArcGIS® using publicly available data. Mastcam image viewsheds locate onto Mars orbital view the terrains that are visible in a given Mastcam image.

options exist for visualizing the Mastcam images that are available online on the PDS in the binary format ".IMG" (Table 1). For example, they are viewable within ArcGIS® (where they can also be converted to other formats), or alternatively, they can be imported in Photoshop as a RAW format, using the information in the label. Here we also provide a script (in Davinci language) that converts multiple MastcamI.MG images into ".TIFF" or ".PNG" or ".JPG" format, which are readable via more basic computer programs. The script requires to have both. IMG images and their associated labels downloaded; its use is detailed in Text S1.

3.1.2. Step 1.2: Create a Map of the Curiosity Rover Traverse in ArcGIS®

Next, in ArcMap, we import the Gale crater orthophoto mosaic, the DEM, and the coordinates of Curiosity's traverse within Gale crater. Step-by-step instructions about importing these datasets into an ArcMap project are provided in Text S2.

3.2. Step 2: Extract and Calculate Mastcam Image Properties

Step 2 consists of extracting and calculating the geometric and geographic properties of the Mastcam image for which to produce a viewshed. These properties will be incorporated into the Viewshed tool in ArcGIS® in Step 3.

3.2.1. Step 2.1: Extract Mastcam Image Geographic Properties

Geographic properties corresponding to the location of the rover at the time the Mastcam image was acquired are present within Mastcam image metadata file: under the subsection "/* Identification Data Elements */", the "**SITE**" and "**DRIVE**" values correspond to this rover location, as expressed in the rover coordinate frame (section 2.2). The Site index increments with successive rover geographic locations, and the Drive index increments every time the rover rolls or steers its wheels. Together, these two values form the rover motion counter (RMC), which is a way of ordering rover activities in time (Deen, 2015; Lakwalla, 2018). To obtain the coordinates corresponding to this location, we use the "Rover path localization table" (Table 1) that for each combination of "Site" and "Drive" values, provides the corresponding Mars latitude and longitude values. ***The metadata file of Mastcam image 1429MR007068017 0702598E01_DRCL indicates a "SITE" value of 56 and a "DRIVE" value of 1,632. In the "Rover path localization table," these values correspond to a "northing" value (latitude) of −277,875.774 m, and a "easting" value (longitude) of 8,141,618.407 m*** (see Text S3).

3.2.2. Step 2.2: Calculate Mastcam Image Geometric Properties

Vertical and horizontal limits of the scan spanned in a given Mastcam image are the geometric properties needed to create a Mastcam image viewshed. Required geometric information includes (1) the fixed field

of view of the Mastcam camera (Right of Left) used to collect the image; (2) the orientation of the Mastcam instrument (the vertical and horizontal angles it was pointing at) when the image was acquired.

First, the Mastcam Right and Left respectively span a fixed field of view (FOV) of 6.8° × 5.1° and 20° × 15° (Bell et al., 2017; Malin et al., 2017): Their horizontal field of view (respectively 6.8° and 20°) corresponds to the view side-to-side view (Figure 3f), and their vertical field of view (respectively 5.1° and 15°) corresponds to the angle of the view up-to-down (Figure 3e). For a given Mastcam image, which of the two Mastcam cameras (Right or Left) was used to collect the image is indicated in the Mastcam data name (section 2.1). ***Mastcam image "1429MR0070680170702598E01_DRCL" corresponds to a Mastcam Right image as indicated by the notation "MR." Thus, its horizontal field of view (hFOV) is 6.8° and its vertical field of view (vFOV) is 5.1°.***

Second, the Mastcam instrument can be pointed vertically and horizontally at variable orientations. The pointing parameters in which a given Mastcam image was acquired are indicated in the Mastcam label file, under the subsection "/* Derived Data Elements */", by the following two parameters:

- The "**FIXED_INSTRUMENT_AZIMUTH**" (Figure 3d) is the horizontal angle (measured positively in the clockwise direction) of the pointing direction of the Mastcam instrument with respect to the North (Malin et al., 2013). An angle of 90° corresponds to a pointing of the camera towards the East.
- The "**FIXED_INSTRUMENT_ELEVATION**" (Figure 3c) is the vertical angle of the pointing direction of the Mastcam instrument. It is measured from the plane which is perpendicular to the local gravity vector and which intersects the elevation axis around which the instrument rotates (Malin et al., 2013). An angle of 0° corresponds to the camera pointing at the horizon (Figure 3c). Positive values correspond to pointing "up," and they increase positively towards zenith. Negative values correspond to pointing towards the ground.

For image 1429MR0070680170702598E01_DRCL, the FIXED_INSTRUMENT_AZIMUTH value indicated in the label is 170.1185, and the FIXED_INSTRUMENT_ELEVATION is 3.3193. This indicates that the Mastcam instrument was pointed at 3.3193° above the horizontal plane, and in a direction South-East, when the image was acquired.

To calculate the orientation of the limits spanned by a given Mastcam image, we first address the vertical limits and second the horizontal limits.

First, the vertical orientation limits of the Mastcam image scan are defined with respect to the horizontal plane and are here called VERT1 and VERT2 (Figure 3e). They are expressed in degrees between 90° and −90°, with positive values representing angles above the horizontal plane. The following equations describe these orientation limits:

$$Vertical\ upper\ limit:\ \ VERT1 = Fixed\_instrument\_elevation + \left(\frac{vFOV}{2}\right) \tag{1}$$

and

$$Vertical\ lower\ limit:\ \ VERT2 = Fixed\_instrument\_elevation - \left(\frac{vFOV}{2}\right) \tag{2}$$

where *vFOV* is the vertical field of view of the Mastcam camera that acquired the image.

For image 1429MR0070680170702598E01_DRCL:

$$VERT1 = Fixed\_instrument\_elevation + \left(\frac{vFOV}{2}\right) = 3.3193 + \left(\frac{5.1}{2}\right) = 5.8693$$

and

$$VERT2 = Fixed\_instrument\_elevation - \left(\frac{vFOV}{2}\right) = 3.3193 - \left(\frac{5.1}{2}\right) = 0.7693$$

The vertical scan limits spanned in this image range from 0.7693° to 5.8693° above the horizontal plane.

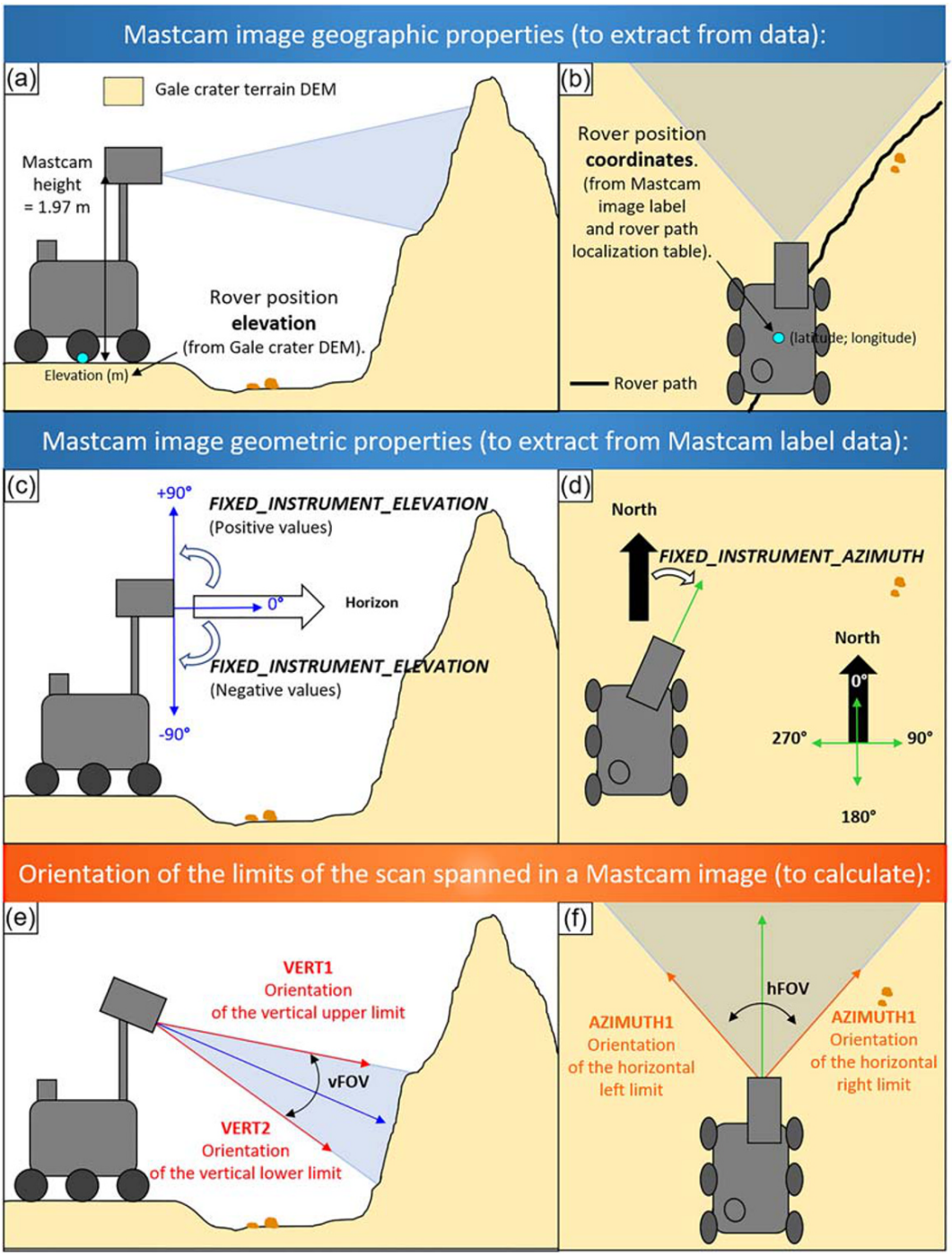

Figure 3. Schematic of the geometric and geographic properties of a Mastcam image used to create the corresponding viewshed. Geographic properties include the rover location's elevation (a) and coordinates at the time the Mastcam image was acquired (b). The fixed instrument elevation (blue arrow) is the vertical angle of the pointing direction of the Mastcam camera (c). The fixed instrument azimuth (green arrow) is the angle of the pointing direction of the Mastcam instrument with respect to the North (c). Mastcam image vertical limits (red arrows) are the angles of the view limits up-to-down (e), and the horizontal limits (orange arrows) are the orientation of the view limits side-to-side (f).

Second, the horizontal angle limits are defined with respect to the North and are here called AZIMUTH1 and AZIMUTH2 (Figure 3f). The sweep proceeds in a clockwise direction from the first azimuth to the second. The values for the angle are given in degrees from 0° to 360°, with 0° representing an orientation North.

$$Horizontal\ left\ limit:\quad AZIMUTH1 = Fixed\_instrument\_azimuth - \left(\frac{hFOV}{2}\right) \tag{3}$$

and

$$Horizontal\ right\ limit:\quad AZIMUTH2 = Fixed\_instrument\_azimuth + \left(\frac{hFOV}{2}\right) \tag{4}$$

where hFOV is the horizontal field of view of the Mastcam camera that acquired the image.

For image 1429MR0070680050702586E01_DRCL:

$$AZIMUTH1 = Fixed\_instrument\_azimuth - \left(\frac{hFOV}{2}\right) = 170.1185 - \left(\frac{6.8}{2}\right) = 166.7185$$

and

$$AZIMUTH2 = Fixed\_instrument\_azimuth + \left(\frac{hFOV}{2}\right) = 170.1185 + \left(\frac{6.8}{2}\right) = 173.5185 \tag{5}$$

The horizontal scan limits spanned in this image range from 166.7185° to 173.5185° with respect to North, which corresponds to a South-East direction.

An excel table template that includes these formulas is provided in Text S4.

3.3. Step 3: Generate the Mastcam Image Viewshed With the ArcGIS® Viewshed Tool

The built-in Viewshed tool in ArcGIS® allows identification of a raster's cells that can be seen from a given observation location (section 2.2). For generating a Mastcam image viewshed, the information required in the ArcGIS® Viewshed tool is as follows:

1. A rater file with topographic information. Here it corresponds to the Gale crater DEM (section 2.2), to provide both the elevation of rover location from where a given Mastcam image was acquired, and the topography of the surrounding terrains (see Text S2).
2. The point observer features. Here this corresponds to a shapefile that includes the coordinates of the rover's location at the time the Mastcam image was acquired (Step 2.1) and the values of the following Viewshed-tool built-in items [ArcGIS® "Using Viewshed and Observer Points for visibility analysis"]:

- OFFSETA: indicates the "vertical distance in surface units to be added to the z-value of the observation point." Here it corresponds to the height of the Mastcam instrument with respect to the Mars ground, that is, 1.97 m (Bell et al., 2017).
- The values VERT1 and VERT2 that define the vertical angle limits to the scan, extracted and calculated in step 2.2. These angles are expressed in degrees between 90 and −90.
- The values AZIMUTH1 and AZIMUTH2 that define the horizontal angle limits to the scan, extracted and calculated in step 2.2. These angles are expressed in degrees from 0 to 360, with 0 oriented to North, and the sweep proceeds in a clockwise direction from the first azimuth to the second.
  Step-by-step instructions for generating a shapefile with these items are presented in Text S5.

Once the viewsheds are generated, their transparency can be turned down, in order to visualize the terrains (Figure 4b, right panel and Figure S5.4).

4. Results and Discussion

Figure 4 shows the viewsheds, generated with this procedure, of the four Mastcam images (acquired on Sol 1429) from Figure 1. Mastcam images 3 and 4 both display terrains that correspond to the top of outcrops,

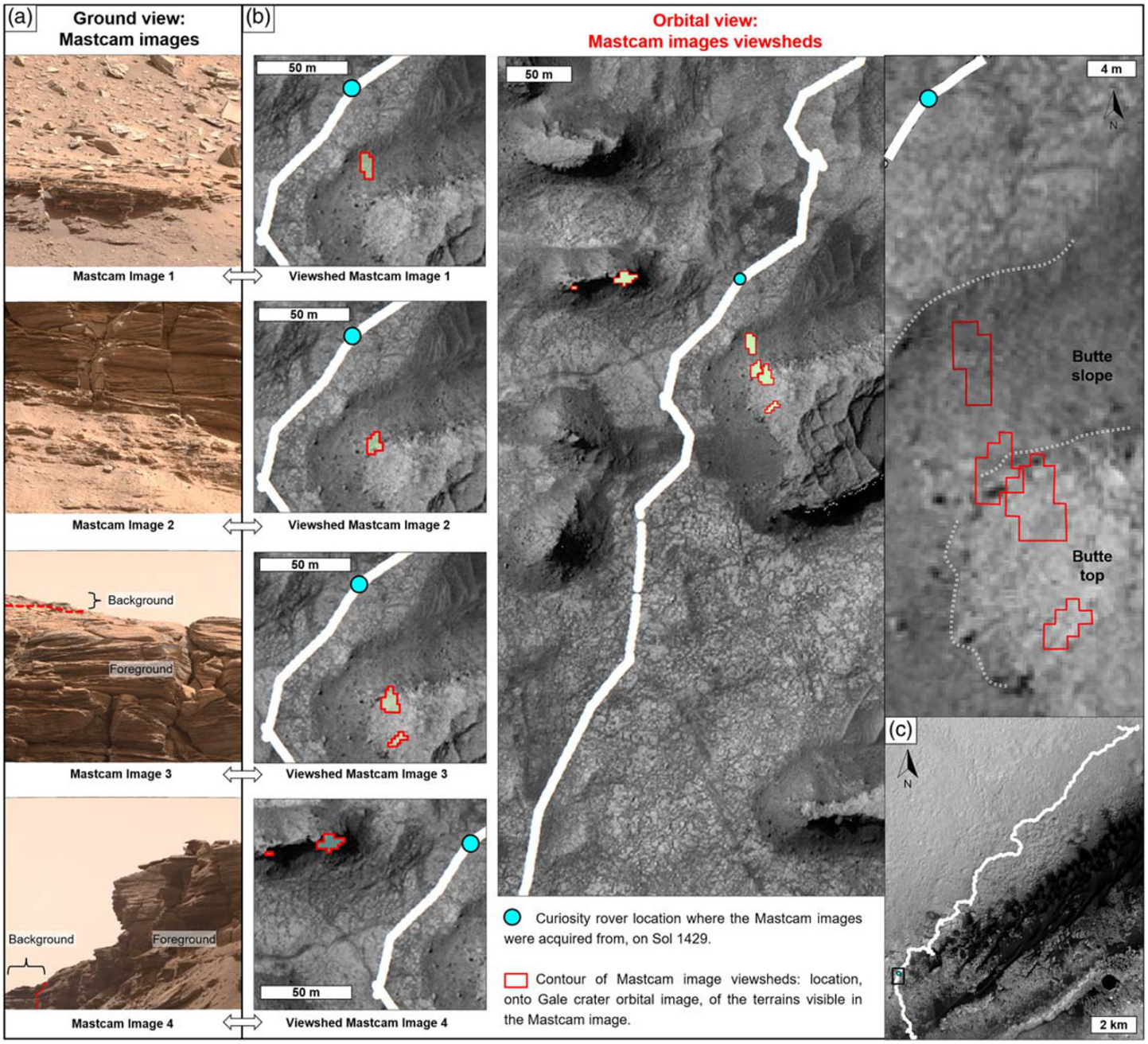

Figure 4. Mastcam image viewsheds (b), generated with the procedure presented here, of four Mastcam images (a) acquired on Sol 1429 (see Figure 1). Viewsheds 3 and 4 are both composed of two areas, because their corresponding Mastcam images each display terrains with "false horizons" (presence of a background and a foreground). (c) Orbital view of the curiosity rover's path.

and their respective viewsheds show they belong to two distinct buttes. This provides an example of how useful these viewsheds can be: Without them, it was not straightforward that the images 3 and 4 correspond to two different outcrops nor was knowing which of the buttes visible from the orbital map these two images correspond to.

Viewsheds of images 1 and 2 are each composed of a single area, while viewsheds of images 3 and 4 are composed of two areas. This is due to the fact that images 3 and 4 both display terrains with "false horizons": A part of the outcrop is present in the image background and is distinct than the one in the foreground (Figure 4). Whereas the terrains in images 1 and 2 do not present a "false horizon."

Moreover, these three viewsheds successfully depict the configuration of images 1 to 3 that correspond to different parts of a butte, from bottom to top (as presented in Figure 1). Viewshed 1 appears downslope and closer to the rover location, compared to the viewsheds of image 2 and 3. Viewshed 1 is located over the butte slope area that in the orbital map appears darker and that corresponds to sand, rockfall, and fractured outcrops. Viewshed 2 is located over the transition from this same butte slope material to the butte top, which in the orbital view appears lighter-toned and corresponds to vertically exposed beds. Viewshed 3 is fully located over the butte top area, above viewshed 2, which is also coherent with the relative configuration of images 2 and 3 presented in Figure 1. Mastcam images 2 and 3 slightly overlap, and this configuration is also captured in their viewsheds (Figures 5a–5b). In the images, the location of the overlap is between the top-left part of Mastcam image 2 and the bottom right part of Mastcam image 3 (Figure 5a), which is also visible in the viewshed configuration (Figure 5b).

Figures 5c–5d show the viewshed of a Mastcam image that shows the same butte as images 2 and 3 do but that was acquired with the Mastcam Left camera (while images 2 and 3 were acquired with the Mastcam Right camera). The lateral extent of the ML viewshed is coherent with the images configuration: The left section of the viewshed extends further left from the viewsheds of the two MR images (Figure 5d), as it does for the respective images (Figure 5c). Figures 5c–5d illustrate that the configuration between the viewshed of ML image with respect to the viewsheds of the two MR images does not fully correspond to the images' relative configuration. Image ML overlaps with a significant portion of MR image 2, and with some of and MR image 3, whereas its viewshed overlaps with that of MRt image 2 but just touches the contact with the viewshed of MR image 3, rather than overlapping with it. Also, the viewshed of ML image shows a ~1 m blank in its middle part (Figure 5d), which does not correspond to what is visible in the image.

Figures 5e–5f show more examples of viewsheds, generated from three images acquired on Sol 1267 (yellow, blue, and white contours) and one acquired on Sol 1272 (red contour). The lateral overlap between images blue and yellow is well captured in their viewsheds. The red image, acquired on Sol 1272, images a portion of the outcrop that was also imaged on Sol 1267 in the blue image: A float rock, visible in both images, is signaled by the white arrow (Figure 5e). This overlap is visible in the relative configuration of the images viewsheds.

In this procedure, aspects we did not take into account include (1) the difference in position on the rover mast of Mastcam Right (MR) and Mastcam Left (ML) cameras (Figure 1c) and (2) the influence of the rover roll (side-to-side tilt) and pitch (front-to-back tilt) at the time the images were acquired. This might explain some of the discrepancies illustrated in Figure 5. Moreover, the precision of the viewsheds also depends on the DEM used to generate them. Here, the Gale crater DEM (section 2.2, Table 1) provides the topography at 1 m/pixel postings (Calef & Parker, 2016). Thus, the precision of the viewshed locations might include errors at the meter scale. Furthermore, the viewsheds are here displayed superposed onto the Gale crater orthophoto mosaic, which has a pixel resolution of 25 cm/pixel (Calef & Parker, 2016) (section 2.2, Table 1). Thus, the precision error of the viewshed is potentially larger than the size of the orthophoto pixels. This needs to be kept in mind when using viewsheds to map onto the orthophoto features smaller than 1–2 m.

One means of assessing the error in this procedure is to measure (in ArcGIS®) the distance between the viewshed and the rover position from where the image was acquired and to compare this distance with the estimated focus distance of the image. In particular, Mastcam images labels include the "BEST FOCUS DISTANCE" parameter, which corresponds to the "estimated distance to best focus from the front of the instrument sapphire window" (Malin et al., 2013). The BEST FOCUS DISTANCE values for Mastcam images 1 to 3 are respectively 19.333, 25.072 and 26.968 m. This increase is consistent with the fact that images 1 to 3 successively correspond to higher parts of the butte, further away from the rover, which is captured by the three viewsheds. As a first order approximation, a hypothesis is that the BEST FOCUS DISTANCE value of a Mastcam image would be similar to the measured distance from the rover position to the center of the image viewshed. We thus generated 14 viewsheds that correspond to Mastcam Right images with BEST FOCUS DISTANCE values ranging from 3.3 to 114.6 m. Each of the 14 viewshed selected correspond to a single area (without foreground and background). For each viewshed, we measured in ArcGIS® the distance between the viewshed centroid and the rover location ($D_{centroid}$). Figures 5g and 5h show the comparison of $D_{centroid}$ values with the BEST FOCUS DISTANCE values (orange points). Also displayed are the corresponding "MINIMUM FOCUS DISTANCE" values (blue points) that specify the

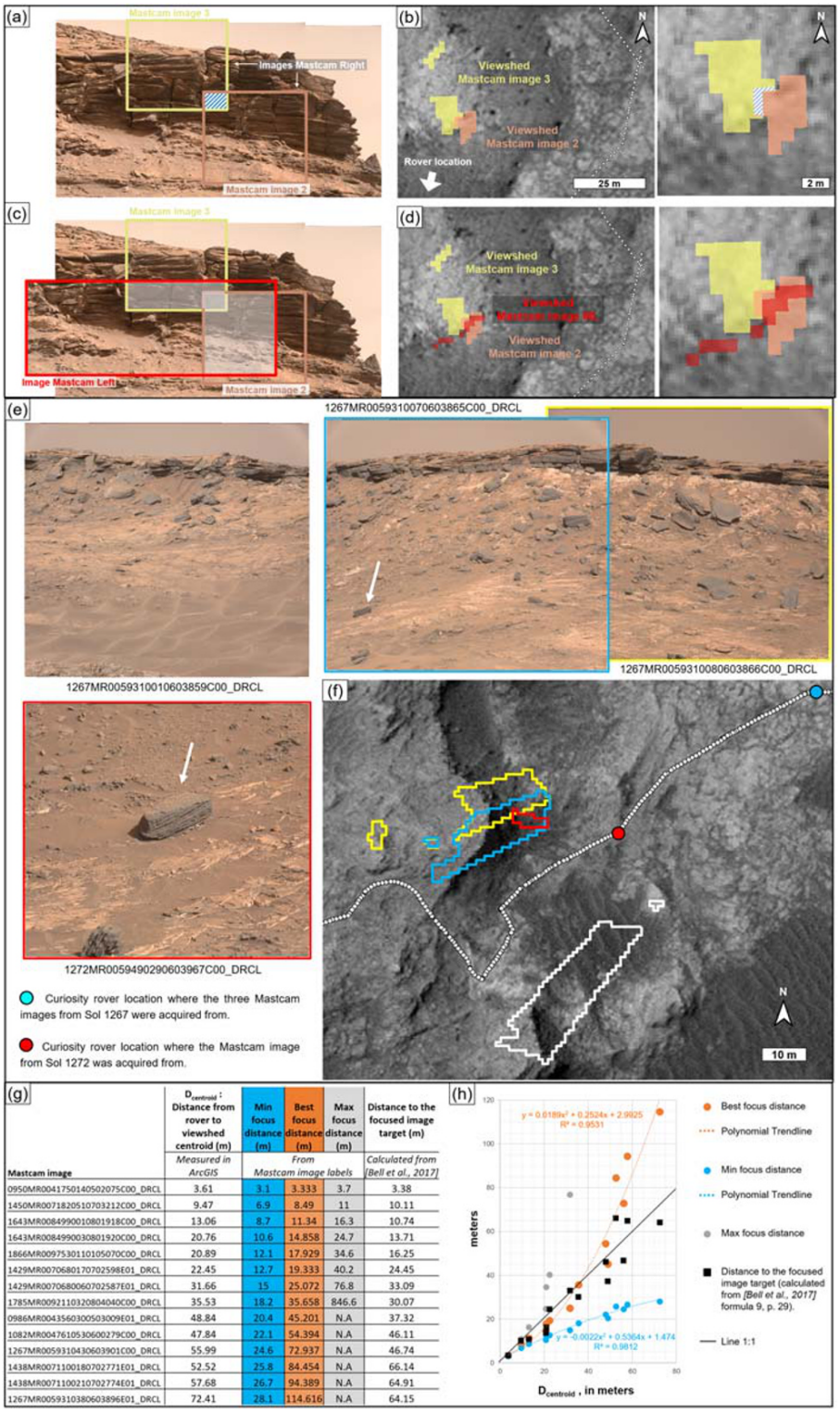

Mastcam image	$D_{centroid}$: Distance from rover to viewshed centroid (m) *Measured in ArcGIS*	Min focus distance (m)	Best focus distance (m)	Max focus distance (m)	Distance to the focused image target (m) *Calculated from [Bell et al., 2017]*
		From Mastcam image labels			
0950MR0041750140502075C00_DRCL	3.61	3.1	3.333	3.7	3.38
1450MR0071820510703212C00_DRCL	9.47	6.9	8.49	11	10.11
1643MR0084990010801918C00_DRCL	13.06	8.7	11.34	16.3	10.74
1643MR0084990030801920C00_DRCL	20.76	10.6	14.858	24.7	13.71
1866MR0097530110105070C00_DRCL	20.89	12.1	17.929	34.6	16.25
1429MR0070680170702598E01_DRCL	22.45	12.7	19.333	40.2	24.45
1429MR0070680060702587E01_DRCL	31.66	15	25.072	76.8	33.09
1785MR0092110320804040C00_DRCL	35.53	18.2	35.658	846.6	30.07
0986MR0043560300503009E01_DRCL	48.84	20.4	45.201	N.A	37.32
1082MR0047610530600279C00_DRCL	47.84	22.1	54.394	N.A	46.11
1267MR0059310430603901C00_DRCL	55.99	24.6	72.937	N.A	46.74
1438MR0071100180702771E01_DRCL	52.52	25.8	84.454	N.A	66.14
1438MR0071100210702774E01_DRCL	57.68	26.7	94.389	N.A	64.91
1267MR0059310380603896E01_DRCL	72.41	28.1	114.616	N.A	64.15

Figure 5. Illustration of precision and accuracy aspects of Mastcam image viewsheds. (a–d) Overlap of viewsheds reproducing the relative configuration of Mastcam image. Orbital maps (b, d) are oriented with North pointing down, to display the outcrop up from the rover location, and thus allow a better comparison of the viewsheds with the Mastcam images (a, c). (e, f) Viewsheds of three images acquired on Sol 1267 (yellow, blue and white contour) and one acquired on Sol 1272. (g, h) Comparison of $D_{centroid}$ distance (measured in ArcGIS®) with the "BEST FOCUS DISTANCE" (from Mastcam labels) and with the "Distance to the focused image target" (calculated from Bell et al., 2017) for viewsheds generated with the procedure.

"estimated distance to the nearest pixel with less than 1 pixel of gaussian blur," and the "MAXIMUM FOCUS DISTANCE" values (gray points) that specify the "estimated distance to the furthest pixel with less than 1 pixel of gaussian blur" (Malin et al., 2013). The $D_{centroid}$ values appear comprised between the corresponding MINIMUM FOCUS DISTANCE and MAXIMUM FOCUS DISTANCE values (Figures 5g and 5h). Figure 5h shows that the relation between $D_{centroid}$ and the BEST FOCUS DISTANCE values is best fit by a second-order polynomial function ($y = 0.0189x^2 + 0.2524x + 2.9925$, with $R^2 = 0.95$). The deviation of $D_{centroid}$ values from this trendline ranges from 0.1 to 7.8 m, with an average of 2.8 m. For most geological applications, such as mapping and measuring outcrops, such average errors are within acceptable limits. These deviations might in part be explained by the intrinsic limitations of the viewsheds procedure (e.g., DEM topography at 1 m/pixel postings) and the parameters not taken into account here (e.g., rover roll and pitch). For example, the largest deviation corresponds to the image with the highest "roll" and "pitch" values (−13.5° and −16.2°, respectively, for image 0986MR0043560300503009E01_DRCL, see Text S6). Also, these distance discrepancies could be related to the fact that the focus distance values from the Mastcam labels are, by definition, estimated distances (Malin et al., 2013).

We also compare the $D_{centroid}$ values with the "distance to the focused image target" as calculated from (Bell et al., 2017, p. 29) (Figures 5g and 5h and Text S6). This calculated distance typically provides a way to estimate distance from the rover to imaged targets in Mastcam images (and thus their spatial scale) and is a function of the Mastcam camera temperature and the focus motor counts (these two parameters being included in the Mastcam image labels) (Bell et al., 2017). The relation between $D_{centroid}$ and the calculated distance to the focused image target values is best fit by a second order polynomial function ($y = -0.0013x^2 + 1.0751x - 2.3646$, with $R^2 = 0.903$), with deviation of $D_{centroid}$ values from this trendline ranging from 0.02 to 17.8 m, with an average of 5.3 m. These deviations might in part be explained by the fact that the calculated distance is a function of the optics temperature (Text S6). Bell et al. (2017) reported that most of the cases where this distance model is not giving as good a fit are for Mastcam Right images "where the actual temperature of the camera could potentially be more than ±5°C different from the reported optics temperature." Another possible cause of distance discrepancy, also reported in Bell et al. (2017), could be for images displaying rocks that only partially fill the field of view (such as image 1450MR0071820510703212C00_DRCL, Figure 5, Text S6), which, combined with the presence of surrounding materials, can cause the autofocus algorithm to lower the focus motor counts relative to other kinds of scenes (Bell et al., 2017).

5. Conclusions and Perspectives

We provide a procedure that locates on Mars orbital view the terrains that are visible in the Curiosity rover Mastcam images. Using the ArcGIS® software and publicly available Mars datasets, this procedure correlates the color high-resolution Mastcam images to the spatially broader orbital context. By coupling ground and orbital views of Gale crater, this procedure can aid in the analysis and interpretation of the geologic terrains along Curiosity rover's route. By utilizing publicly available Mars datasets, this procedure is accessible and can be used with current as well as future publicly released Mastcam images. In addition, this procedure can be used as pedagogic material by the Geosciences or Planetary Sciences community, for teaching these important concepts, and enhancing students' skillsets in GIS. Additionally, the implementation of this procedure in classrooms can provide students with experience working with both Mars orbital and rover datasets.

Future work includes automating aspects of this procedure, in particular to extract and calculate the properties of Mastcam images (Steps 2 of section 3), and accelerate the generation of multiple viewsheds. An additional perspective is to generate viewsheds of Mastcam mosaics (such as the one presented in Figure 1a) rather than viewsheds of individual Mastcam images. Also, further improving the precision of the viewsheds (e.g., by taking into account the rover roll and pitch). Future work also includes adapting the procedure to an open-source GIS software (e.g., QGIS), in order to further enhance the accessibility of this Mastcam images viewshed procedure.

Data Availability Statement

The data used in this work are publicly available: Sources are compiled in Table 1.

Acknowledgments

We are grateful to the MSL engineers and scientists, in particular the Mastcam Team, and to the PDS teams, thanks to whom such awesome Mars datasets are acquired and made available. We thank Dr. Fred J. Calef III and an anonymous reviewer for their thorough reviews and thoughtful comments that improved this manuscript. The open access publishing fees for this article have been covered by the Texas A&M University Open Access to Knowledge Fund (OAKFund), supported by the University Libraries.

References

"MSL Coordinate Systems for Science Instruments." (2013). https://an.rsl.wustl.edu/msl/mslbrowser/an3.aspx

Arvidson, R. E., DeGrosse, P., Grotzinger, J. P., Heverly, M. C., Shechet, J., Moreland, S. J., et al. (2017). Relating geologic units and mobility system kinematics contributing to Curiosity wheel damage at Gale Crater, Mars. *Journal of Terramechanics*, *73*, 73–93. https://doi.org/10.1016/j.jterra.2017.03.001

Banham, S. G., Gupta, S., Rubin, D. M., Watkins, J. A., Sumner, D. Y., Edgett, K. S., et al. (2018). Ancient Martian aeolian processes and palaeomorphology reconstructed from the Stimson Formation on the lower slope of Aeolis Mons, Gale Crater, Mars. *Sedimentology*, *65*, 993–1042. https://doi.org/10.1111/sed.12469

Bell, J. F., Godber, A., McNair, S., Caplinger, M. A., Maki, J. N., Lemmon, M. T., et al. (2017). The Mars science laboratory Curiosity rover Mastcam instruments: Preflight and in-flight calibration, validation, and data archiving. *Earth and Space Science*, *4*, 396–452. https://doi.org/10.1002/2016EA000219

Bridges, N. T., Sullivan, R., Newman, C. E., Navarro, S., van Beek, J., Ewing, R. C., et al. (2017). Martian aeolian activity at the Bagnold Dunes, Gale Crater: The view from the surface and orbit. *Journal of Geophysical Research: Planets*, *122*, 2077–2110. https://doi.org/10.1002/2017JE005263

Calef, F. J. III, & Parker, T. (2016). MSL Gale merged orthophoto mosaic. PDS Annex, U.S. Geological Survey. Available at http://bit.ly/MSL_Basemap

Deen, R. (2015). Mars Science Laboratory Software Interface Specification. *PLACES Data Products for PDS*, https://pds-imaging.jpl.nasa.gov/data/msl/MSLPLC_1XXX/DOCUMENT/

Dickson, J. L., Kerber, L. A., Fasett, C. I., & Ehlmann, B. L. (2018). A global, blended CTX mosaic of Mars with vectorized seam mapping: A new mosaicking pipeline using principles of non-destructive image editing. Paper presented at 49th Lunar and Planetary Science Conference. Abstract 2480. Retrieved from http://murray-lab.caltech.edu/CTX/LPSC2018_CTX-Mosaic-Poster.pdf

Ewing, R. C., Lapotre, M. G. A., Lewis, K. W., Day, M., Stein, N., Rubin, D. M., et al. (2017). Sedimentary processes of the Bagnold Dunes: Implications for the eolian rock record of Mars. *Journal of Geophysical Research: Planets*, *122*, 2544–2573. https://doi.org/10.1002/2017JE005324

Golombek, M., Grant, J., Kipp, D., Vasavada, A., Kirk, R., Fergason, R., et al. (2012). Selection of the Mars science laboratory landing site. *Space Science Reviews*, *170*(1-4), 641–737. https://doi.org/10.1007/s11214-012-9916-y

Gong, W. (2015). Discussions on localization capabilities of MSL and MER rovers. *Annals of GIS*, *21*(1), 69–79. https://doi.org/10.1080/19475683.2014.992367

Grotzinger, J. P., Gupta S., Malin M. C., Rubin D. M., Schieber J., Siebach K., et al. (2015). Deposition, exhumation, and paleoclimate of an ancient lake deposit, Gale crater, Mars. *Science*, *350*(6257), aac7575–aac7575. https://doi.org/10.1126/science.aac7575

Lakwalla, E. (2018). *The design and engineering of curiosity: How the Mars rover performs its job*. Berlin, Germany: Springer International Publishing. https://doi.org/10.1007/978-3-319-68146-7

Le Deit, L., Mangold, N., Forni, O., Cousin, A., Lasue, J., Schröder, S., et al. (2016). The potassic sedimentary rocks in Gale Crater, Mars, as seen by ChemCam on board curiosity. *Journal of Geophysical Research: Planets*, *121*, 784–804. https://doi.org/10.1002/2015JE004987

Lewis, K. W., & Turner, M. L. (2019). Geologic structure of the Vera Rubin Ridge, Gale Crater, Mars. Paper presented at 50th Lunar and Planetary Science Conference. Retrieved from https://www.hou.usra.edu/meetings/lpsc2019/pdf/2216.pdf

Malin, M. C., Edgett, K. S., Jensen, E., #x00026; Lipkaman, L. (2013). Mars Science Laboratory Project Software Interface Specification (SIS): Mast camera (Mastcam), Mars Hand Lens Imager (MAHLI), and MARs Descent Imager (MARDI) experimental data record (EDR) and reduced data record (RDR) PDS data products. Retrieved from http://pds-imaging.jpl.nasa.gov/data/msl/MSLMST_0001/DOCUMENT/

Malin, M. C., Ravine, M. A., Caplinger, M. A., Ghaemi, F. T., Schaffner, J. A., Maki, J. N., et al. (2017). The Mars science laboratory (MSL) mast cameras and descent imager: Investigation and instrument descriptions. *Earth and Space Science*, *4*, 506–536. https://doi.org/10.1002/2016EA000252

McEwen, A. S., & the HiRISE Science and Operations Team. (2018). "The Future of MRO/HiRISE" MEPAG Meeting 36, April 2018. https://mepag.jpl.nasa.gov/meeting/abstracts/McEwen_HiRISEfuture.pdf

McLennan, S. M., Bell, J. F., Anderson, R. B., Calef, F., Bridges, J. C., Campbell, J. L., et al. (2014). Elemental geochemistry of sedimentary rocks at Yellowknife Bay, Gale Crater, Mars. *Science*, *343*, 1244734. https://doi.org/10.1126/science.1244734

Nachon, M., Mangold, N., Forni, O., Kah, L. C., Cousin, A., Wiens, R. C., et al. (2017). Chemistry of diagenetic features analyzed by ChemCam at Pahrump Hills, Gale Crater, Mars. *Icarus*, *281*, 121–136. https://doi.org/10.1016/j.icarus.2016.08.026

Parker, T. J., Malin, M. C., Calef, F. J., Deen, R. G., Gengl, H. E., Golombek, M. P., et al. (2013). Localization and 'contextualization' of Curiosity in Gale Crater, and other landed mars missions. Paper presented at 44th Lunar and Planetary Science Conference. Abstract 2534. Retrieved from https://www.lpi.usra.edu/meetings/lpsc2013/pdf/2534.pdf

Quinn, D. P., & Ehlmann, B. L. (2019). A PCA-based framework for determining remotely sensed geological surface orientations and their statistical quality. *Earth and Space Science*, *6*, 1378–1408. https://doi.org/10.1029/2018EA000416

Stack, K. M., Edwards, C. S., Grotzinger, J. P., Gupta, S., Sumner, D. Y., Calef, F. J., et al. (2016). Comparing orbiter and rover image-based mapping of an ancient sedimentary environment, Aeolis Palus, Gale Crater, Mars. *Icarus*, *280*, 3–21. https://doi.org/10.1016/j.icarus.2016.02.024

Stein, N., Grotzinger, J. P., Schieber, J., Mangold, N., Hallet, B., Newsom, H., et al. (2018). Desiccation cracks provide evidence of lake drying on Mars, Sutton Island Member, Murray Formation, Gale Crater. *Geology*, *46*, 515–518. https://doi.org/10.1130/G40005.1

Stein, N. T., Quinn, D. P., Grotzinger, J. P., Fedo, C., Ehlmann, B. L., Stack, K. M., et al. (2020). Regional structural orientation of the Mt. Sharp group revealed by in-situ dip measurements and stratigraphic correlations on the Vera Rubin Ridge. *Journal of Geophysical Research: Planets*, *125*, e2019JE006298. https://doi.org/10.1029/2019JE006298

Sun, V. Z., Stack, K. M., Kah, L. C., Thompson, L., Fischer, W., Williams, A. J., et al. (2019). Late-stage diagenetic concretions in the Murray Formation, Gale Crater, Mars. *Icarus*, *321*, 866–890. https://doi.org/10.1016/j.icarus.2018.12.030

Thompson, L. M., Schmidt, M. E., Spray, J. G., Berger, J. A., Fairén, A. G., Campbell, J. L., et al. (2016). Potassium-rich sandstones within the Gale impact crater, Mars: The APXS perspective. *Journal of Geophysical Research: Planets*, *121*, 1981–2003. https://doi.org/10.1002/2016JE005055

Wiens, R. C., Rubin, D. M., Goetz, W., Fairén, A. G., Schwenzer, S. P., Johnson, J. R., et al. (2017). Centimeter to decimeter hollow concretions and voids in Gale crater sediments, Mars. *Icarus*, *289*, 144–156. https://doi.org/10.1016/j.icarus.2017.02.003